International Journal of Scientific Engineering and Technology (ISSN : 2277-1581)
Volume No.3 Issue No.12, pp : 1449-1454 01 Dec. 2014

MEMS Based Microneedle Actuator with Piezoresistive Force Feedback System for Biomedical Applications

Ashen Wijesiri, Y.W.R. Amarasinghe
Department of Mechanical Engineering, University of Moratuwa, Moratuwa, Sri Lanka
ashenrandika@gmail.com

Abstract*: This paper presents a novel design of MEMS based microneedle actuator with force feedback system which can be used for biomedical applications such as cell manipulation, drug delivery and DNA injection. The actuation mechanism of microneedle is driven by two electrostatic comb actuators. Since the manipulated objects are very sensitive, and can be easily damaged, it's essential to have a force feedback system in the micro actuator to avoid unnecessary deformations. Piezoresistive sensing elements are used for the force feedback of the system. The proposed system was simulated using COMSOL Multiphysics software considering the anisotropic material properties and the nonlinear behavior of coupled physics. Different configurations of force sensing elements were simulated to identify most suitable configuration with higher resolution.

***Keywords*—MEMS; Electrostatic; Piezoresisitve; Micro Manipulation; Force Feedback**

I. INTRODUCTION

During last few years, the interest on the manipulation of objects on the micro/nano scale has been increased dramatically and its growth is continuing across wide range of fields: biological and biomedical research, microelectromechanical systems, and microelectronics devices [1]. Special tools termed micromanipulators are being developed which have the capability of grasping, pushing, pulling, positioning, orienting, and bending with sub micrometer precision [2]. Since conventional manufacturing technologies are not capable of fabricating such micro scaled devices, MEMS technology is introduced to develop such systems. MEMS devices are manufactured using micro fabrication techniques which were derived from the VLSI technologies [3]. But these devices have mechanically moving components that involves with different types of physical phenomena such as structural mechanics, electrostatics, piezoelectricity, and piezoresistivity etc.

There are many challenges in designing, manufacturing, and operating of the micro manipulators. Specially, biological cells and bio materials are very sensitive and likely to damage. Therefore, the micro manipulators should be able to provide precise movements and regulate the applied forces at sub micro newton scale. Also force feedback is necessary to avoid any damages or deformations during the manipulation process [4].

At present, a number of researchers have developed different types of micromanipulation systems for biological sample manipulation, based on different types of actuation and sensing principles. Alogla et al. [5] made a microgripper which can be actuated using pneumatic pressure exerted by a syringe. The operating range of the gripper is 200µm to 2mm, which is not enough for small objects like biological cells. Beyeler et al [4] demonstrated a silicon based, monolithically fabricated microgripper for manipulating biological cells. The electrostatically actuated gripper is able to handle objects having dimension up to 100µm. Capacitive force sensors are used for the force feedback system. It's known that these type of sensors are inherently nonlinear and as the sensors are scaled down, parasitic capacitance is introduced and it affects the accuracy of the sensors [6]. Chen et al. [7] have demonstrated a piezoelectrically driven microgripper with sidewall piezoresistive sensors. It can handle wide range of objects from 25µm to 80µm with real time gripping force feedback. The sensitivity of the sensors was more than 72V/N. Use of piezoelectric material complicates the manufacturing process of the actuator. Also the fabrication process of the non-conventional sidewall piezoresistor is pretty complicated. Messenger et al. [8] developed a MEMS thermal actuator which is having maximum displacement of 10µm. Thermal expansion of the silicon is used as the actuation principle. It's known that thermal actuator consumes relatively large amount of power [9] and it's sensitive to environmental temperature changes [10]. Also the response time of the thermal actuators are relatively high compared to other actuation mechanisms [11].

This paper presents a novel design and the simulation of MEMS based microneedle, with electrostatic actuation and piezoresistive force sensing. It was identified that electrostatic actuators are simple to fabricate, consume low power and has fast actuation response compared to other actuation mechanisms. With piezoresistive force sensing elements, it's possible to achieve high sensitivity and they are easy to fabricate. The proposed system will be having the capability of cell manipulation for biomedical applications such as cell penetration testing, drug delivery, and DNA injection. Electrostatic comb actuators will be used as the actuating mechanism of the needle. Piezoresistive sensing elements are integrated into the mechanism to provide the force sensing capability.

PROPOSED MICRONEEDLE ACTUATOR WITH FORCE FEEDBACK SYSTEM

Fig. 1 shows the model of the proposed design of microneedle actuator. The structure can be fabricated using silicon-on-insulator- (SOI) wafer. The whole mechanism consists of electrostatic comb drives, fixed-fixed type springs, and piezoresistive sensing elements.

A. Electrostatic Combdrive Actuator

International Journal of Scientific Engineering and Technology (ISSN : 2277-1581)
Volume No.3 Issue No.12, pp : 1449-1454 01 Dec. 2014

The electrostatic comb drive consists of two parts called stator and rotor. Stator is stationary comb and fixed onto the silicon base structure. Rotor is the moving at the lateral direction to the stator comb. Fingers of the rotor are interdigitated with the stator. Longitudinal combdrives, which the direction of the relative movement between stator and rotor is along the longitudinal axis, used to obtain higher displacement of the micro needle.

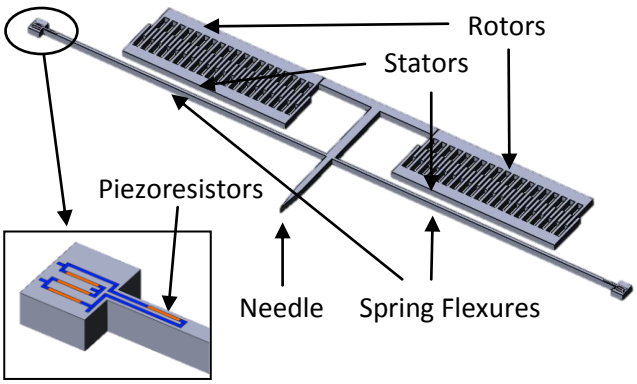

Fig. 1. Proposed design of the microneedle actuator

Single finger of a comb drive is shown in Fig. 2. The structure is approximated as a parallel plate model between the interdigitated parts of the comb fingers. The capacitance between the stator and the rotor is given by (1),

$$C = \frac{2n\varepsilon_0 hy}{d} \quad (1)$$

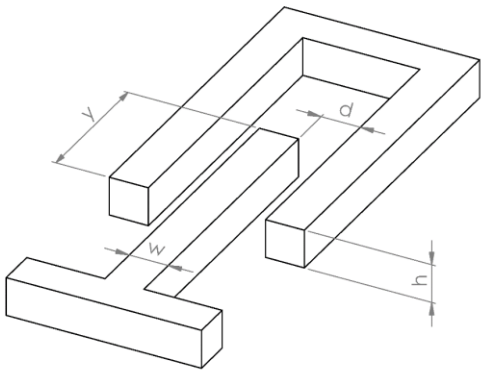

Fig. 2. Single finger of a comb drive

Where n is the number of fingers, ε_0 is the permittivity of air, h is the height of the comb fingers, y is the initial overlap of comb fingers, d is the gap between the fingers. The electrostatic force in the y-direction is given by,

$$F = \frac{n\varepsilon_0 hV^2}{d} \quad (2)$$

Where V is the applied voltage between stator and rotor. The capacitance between the pair of the fingers is contributed by both the vertical surfaces of the fingers and the fringe capacitance fields. The fringe capacitance is difficult to calculate analytically [12]. The significance of the fringe fields in increased as the dimension become smaller. Therefore Finite Element Analysis (FEA) was performed to obtain accurate results.

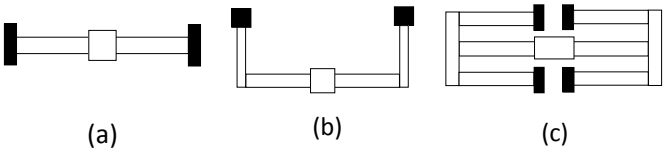

Fig.3. Different types of spring flexures (a) fixed-fixed, (b) crab leg and (c) folded flexure

B. Restroing Mechanism of Combdrive Actuator

The displacement of the rotor is controlled by a balance between the electrostatic force and the mechanical restoring force of the spring flexures. Mechanical forces are produced by the spring flexures. Different types of spring flexures such as, fixed-fixed, crab leg, and folded flexure can be used with electrostatic comb actuators (fig. 3) [13]. Fixed-fixed spring flexures (fig.4) are used in this design due to its high stiffness ratio [13]. The flexures are deflected as the electrostatic force (F) is applied.

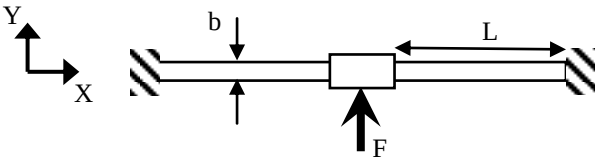

Fig.4. Fixed-fixed spring flexures

The spring constants for x and y directions of the flexure is given by (3) and (4) respectively,

$$k_x = \frac{2Ebh}{L} \quad (3)$$

$$k_y = \frac{2Ebh^3}{L^3} \quad (4)$$

Where, E is the Young's modulus, b, h and L are the width, height, and length of the spring respectively. As the flexures are deflected, stress is introduced. The maximum strain and stress are occurred at the fixed ends of the flexures. The maximum strain is given by (5),

$$\varepsilon_{max} = \frac{FLh}{4EI} \quad (5)$$

The maximum stress is given by (6),

$$\sigma_{max} = \frac{FLh}{2I} \quad (6)$$

It's desired to locate the force sensing elements where the stress are maximum. Therefore the force sensors were located near the fixed ends of the springs.

C. Anisotropic Properties of Silicon

The proposed microneedle actuator can be fabricated using Silicon. It's the most common single material used in MEMS fabrication [14].Silicon is an anisotropic material. Its properties depend on the orientation relative to the crystal lattice. Therefore

to obtain accurate results, the anisotropic properties of the silicon were used for the simulation. It was considered that the system is fabricated using n-type lightly doped (100) silicon wafer. The [110] crystal axes of the silicon is aligned with the longitudinal direction of the spring flexure. The material properties are listed in table 1.

TABLE 1 MATERIAL PROPERTIES OF SILICON [14]

Parameter	Value
Elastic modulus	E_1 = 165.7 GPa, E_2 = 63.9 GPa, E_3 = 79.6 GPa
Poisson ratio	$\nu_{12} = \nu_{13} = \nu_{23} = 0.278$
Shear modulus	$G_{12} = G_{13} = G_{23}$ = 79.64 GPa

D. Piezoresistive force feedback system

Piezoresistivity of the silicon is used as the sensing principle of the force sensors. Piezoresistors are very sensitive and easy to fabricate compared to other sensing methods available for micro manipulators. The resistivity of the piezoresistors change with the applied stress. If the x, y and z axes are aligned with the <100> crystal axes of the silicon, the resistivity varies with applied stress according to (7),

$$\begin{pmatrix}\rho_1\\ \rho_2\\ \rho_3\\ \rho_4\\ \rho_5\\ \rho_6\end{pmatrix} = \begin{pmatrix}\rho_0\\ \rho_0\\ \rho_0\\ 0\\ 0\\ 0\end{pmatrix} + \rho_0 \begin{pmatrix}\pi_{11} & \pi_{12} & \pi_{12} & 0 & 0 & 0\\ \pi_{12} & \pi_{11} & \pi_{12} & 0 & 0 & 0\\ \pi_{12} & \pi_{12} & \pi_{11} & 0 & 0 & 0\\ 0 & 0 & 0 & \pi_{44} & 0 & 0\\ 0 & 0 & 0 & 0 & \pi_{44} & 0\\ 0 & 0 & 0 & 0 & 0 & \pi_{44}\end{pmatrix} \begin{pmatrix}T_1\\ T_2\\ T_3\\ T_4\\ T_5\\ T_6\end{pmatrix} \quad (7)$$

Where, T is the applied stress, ρ_0 is isotropic resistivity of the unstressed crystal and the terms π_{ij} are the components of the piezoresistive tensor. The piezoresistive components π_{11},π_{12} and π_{44} varies with the doping concentration, type of dopant, and the operating temperature.

The thickness of the piezoresistor is negligible compared to its length and width. According to the configuration of the piezoresistor, the direction of the applied strain is <110>. And the directions of the current flows are <110> and <1$\bar{1}$0>. The piezoresistive coefficients of the piezoresistor can be derived as (8) and (9),

$$\pi'_{11} = (\pi_{11} + \pi_{12} + \pi_{44})/2 \quad (8)$$

$$\pi'_{12} = (\pi_{11} + \pi_{12} - \pi_{44})/2 \quad (9)$$

Therefore the change of the resistance of the piezoresistor ($\Delta R/R$) can be calculated as (10),

$$\frac{\Delta R}{R} = \frac{\sigma_1(\pi_{11}+\pi_{12}-\pi_{44})}{2} + \frac{\sigma_2(\pi_{11}+\pi_{12}-\pi_{44})}{2} \quad (10)$$

Where σ_1 and σ_2 are the two stress components. Piezoresistivity components of the p-type single crystal silicon was taken as follows,

TABLE 2 PIEZORESISTIVITY COMPONENTS OF P-TYPE SINGLE CRYSTAL SILICON

Piezoresistance coefficient (10^{-11} Pa^{-1})	p-type (resistivity = 7.8 Ω cm)
π_{11}	6.6
π_{12}	-1.1
π_{44}	138.1

Piezoresistors are very sensitive to the environmental temperature changes. Therefore Wheatstone bridge configuration is used to eliminate those disturbances and to obtain an accurate readings.

We have tested the Wheatstone bridge with both quarter-bridge and half bridge configuration (Fig. 5).

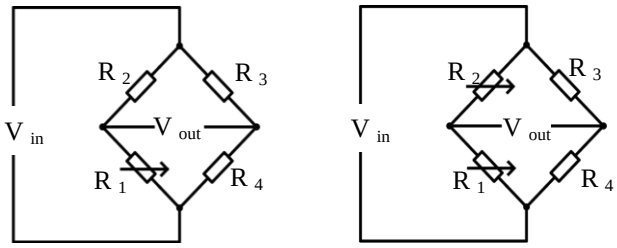

Fig. 5. Wheatstone bridge with (a) quarter-bridge and (b) half bridge configuration

Fig. 5(a) shows the quarter bridge configuration. R_1 is the force sensing piezoresistor located on the spring flexure, which is subjected to tension. Other piezoresistors are located on the rigid substrate where they are not subjected to any stresses. The relationship between the input voltage (V_{in}) and the output voltage (V_{out}) is given by (11),

$$V_{out} = \left(\frac{R_2}{R_1+R_2} - \frac{R_4}{R_3+R_4}\right)V_{in} \quad (11)$$

Since all the dimension and properties of all the piezoresistors are same, the initial resistance of the piezoresistors are identical. Also the resistance of the sensing piezoresistor can be given by (12),

$$R_1 = R + \Delta R \quad (12)$$

Therefore the output voltage of the quarter bridge is given by (13),

$$V_{out} = \frac{1}{2}\left(\frac{-\frac{\Delta R}{R}}{2+\frac{\Delta R}{R}}\right)V_{in} \quad (14)$$

Fig. 5(b) shows the half bridge configuration. R_1 and R_2 sensors are located on the spring flexure and they are subjected to tension and compression respectively. Since all the dimension and properties of all the piezoresistors are same, the initial resistance of the piezoresistors are identical. Both R_1 and R_2 are subjected to same magnitude of tension and compression, and their change of resistance are given by (15) and (16),

$$R_1 = R + \Delta R \quad (15)$$

$$R_2 = R - \Delta R \quad (16)$$

Therefore the output voltage of the half bridge is given by (17),

$$V_{out} = \frac{1}{2}\left(\frac{-\Delta R}{R}\right) V_{in} \quad (17)$$

II. Coupled Field Finite Element Analysis of the Design

The operating behavior of the proposed system is a direct result of several types of physical phenomena such as, structural mechanics, electrostatics and piezoresistivity. The coupling of these different kind of physics, with considerations associated with their micro scaled dimensions, poses significant challenges to the analysis of the proposed design. Therefore finite element analysis (FEA) software COMSOL Multiphysics was used to simulated the design.

Following parameters were used for the electrostatic combdrive actuator.

TABLE 3 PARAMETERS OF THE COMBDRIVE ACTUATOR

Parameter	Value
Number of fingers	40
Length of fingers	50µm
Width of fingers	5µm
Gap between fingers	2µm
Height of fingers	10µm
Initial overlap of fingers	25µm

The length, width and height of the spring flexure was taken as 500µm, 5µm and 10µm respectively (Fig. 6).

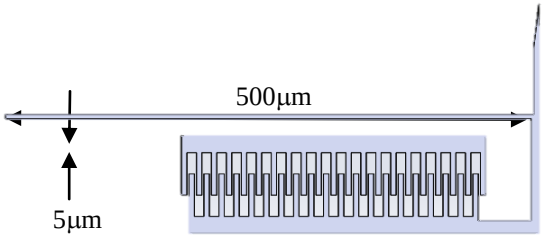

Fig. 6. Spring flexure dimension

The actuation voltage of the simulated comb drive was varied from 50V to 200V by steps of 10V. Applied voltage vs. displacement of the needle is shown in Fig. 7. The stress distribution of the structure for the actuation voltage of 100V, is shown in Fig. 8.

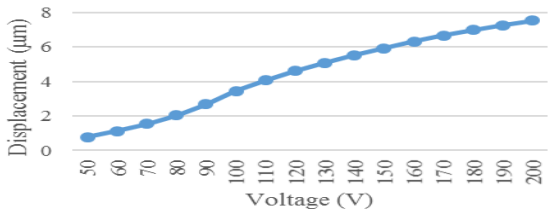

Fig. 7. Voltage vs. displacement

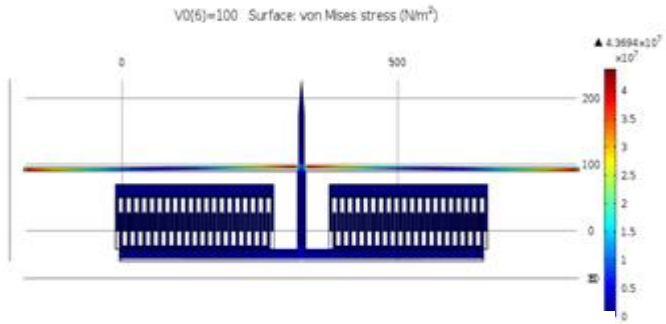

Fig. 8. Stress distribution of the structure

The simulation results confirms that the maximum stresses are produced at the fixed ends of the spring flexures. Stress distribution along the spring flexure was analyzed to find the optimum location to place the piezoresistive force sensor. The variation of the stress along the spring flexure with the actuation voltage, is shown in Fig. 9.

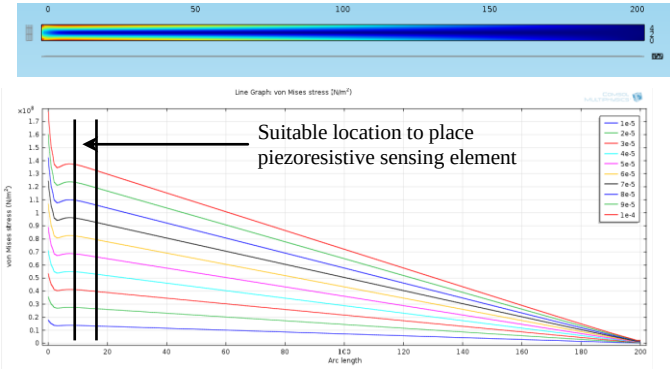

Fig. 9. Variation of the stress along the spring flexure

It was observed that the highest stress point is occurred at the fixed end of the spring flexure. But the piezoresistors always have finite length of at least of 10µm, so that it's not possible to place the piezoresistor at that single point. It was identified that the region of 10µm long, at the distance of 8µm from the fixed end, is suitable for locating the sensing element.

P-type slightly doped silicon is used for the piezoresistive sensors and the conductive regions of the resistor bridge (Fig. 10). The doping concentrations of the piezoresistors and the conductive regions, was taken as $1x10^{19}$ cm^{-3} and $1.5x10^{20}$ cm^{-3} respectively. The surface thickness of both piezoresistors and the conductive layers, was taken as 200nm.

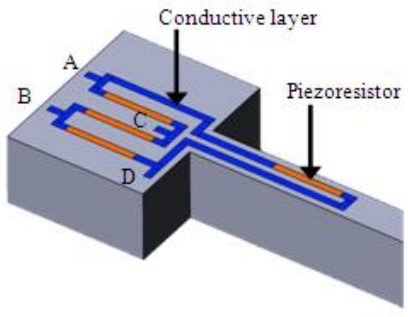

Fig. 10. Quarter-bridge configuration of piezoresistors

Input voltage of 3V was applied to the A and B input terminals of the Wheatstone bridge. Output voltage between the C and D out terminals, was measured as the actuation voltage of the comb drive was varied. The current flow and the voltage gradients of the Wheatstone bridge configurations are is shown in Fig. 11(a) and 11(b). Output voltage of the Wheatstone bridge vs. actuation voltage is shown in Fig.12

The output of the quarter bridge varies from 9.64mV to 11.64mV of 2mV range and for the half bridge it varies from 1.44mV to 4.99mV of 3.55mV range. Therefore it was identified that the half bridge configuration gives better resolution than the quarter bridge configuration.

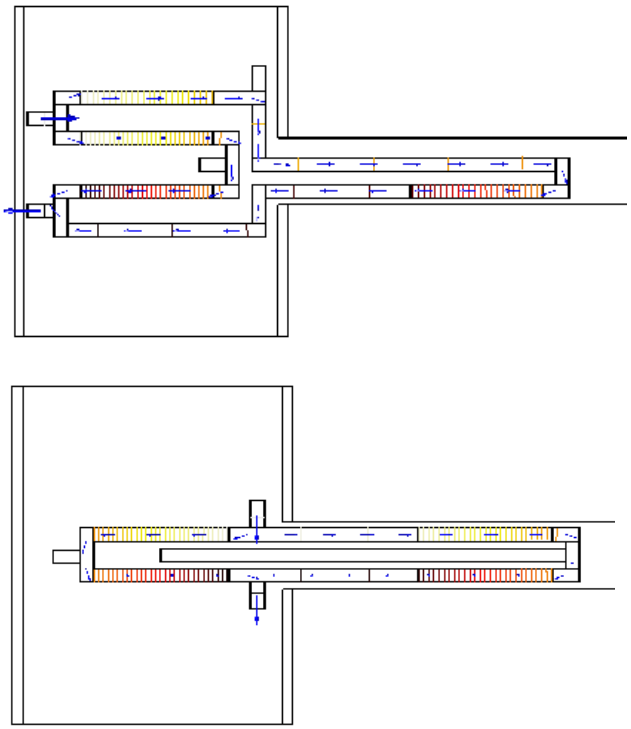

Fig. 11. Current flow and voltage gradients of (a) quarter-bridge (b) half bridge

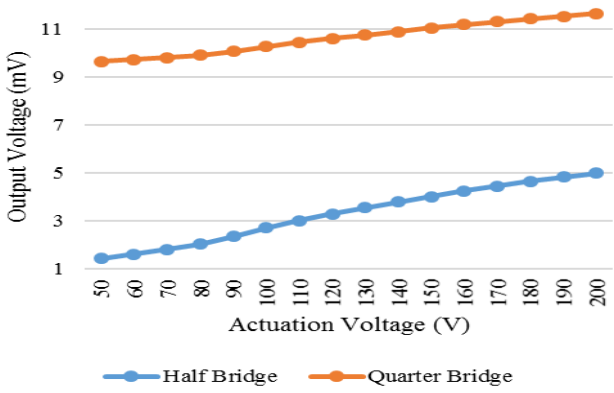

Fig. 12. Output voltage of the Wheatstone bridge vs. actuation voltage

The overview of the proposed experimental setup of the system is shown in Fig. 13. The Microneedle actuator and sensory feedback system will be packaged in a single package. Power will be supplied via a DC power supply and it will be regulated by the voltage regulator. The sensory feedback of the microneedle will be observed using the oscilloscope. The visual feedback of the operation will be captured by the camera which will be connected to the microscope and it will be displayed on the computer screen. The actuation voltage of the micro actuator will be controlled according to the force feedback and the visual feedback.

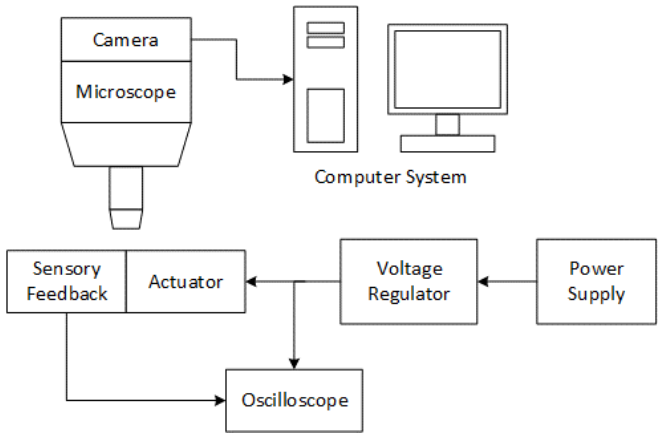

Fig. 13. Overview of the proposed experimental setup

III. Conclusion

Electrostatically actuated microneedle actuator with force feedback system was designed and simulated in this research. The maximum displacement of the simulated design was 7.5µm for the maximum actuation voltage of 200V. The minimum displacement of the actuator is 40nm/V. The piezoresistive effect was used as the force sensing principle of the actuator. Two types of piezoresistor configurations were simulated. Output resolution of the half bridge configuration was 0.02mV/V according the simulation results. The design of the microneedle actuator is well suited for the biomedical applications.

REFERENCES

i. *M. Gauthier and S. Régnier, Robotic Micro-Assembly. New York, NY, USA: Wiley-IEEE Press, 2010.*

ii. *N. Chronis and L. P. Lee, "Electrothermally activated SU-8 microgripper for single cell manipulation in solution," J. Microelectromechanical Syst., vol. 14, no. 4, pp. 857–863, Aug. 2005.*

iii. *A. C. R. Grayson, R. S. Shawgo, A. M. Johnson, N. T. Flynn, Y. Li, M. J. Cima, and R. Langer, "A BioMEMS Review: MEMS Technology for Physiologically Integrated Devices," Proc. IEEE, vol. 92, no. 1, pp. 6–21, Jan. 2004.*

iv. *F. Beyeler, A. Neild, S. Oberti, D. J. Bell, Y. Sun, J. Dual, and B. J. Nelson, "Monolithically fabricated microgripper with integrated force sensor for manipulating microobjects and biological cells aligned in an ultrasonic field," J. Microelectromechanical Syst., vol. 16, pp. 7–15, 2007.*

v. *a. Alogla, P. Scanlan, W. M. Shu, and R. L. Reuben, "A Scalable Syringe-Actuated Microgripper for Biological*

Manipulation," Sensors Actuators A Phys., vol. 202, pp. 135–139, Nov. 2013.

vi. P. Rantakari, J. Kiihamaki, M. Koskenvuori, T. Lamminmaki, and I. Tittonen, "Reducing the Effect of Parasitic Capacitance on MEMS Measurements," in IEEE International Solid-State Sensors and Actuators Conference (Transducers), 2001, pp. 1–4.

vii. T. Chen, L. Chen, and L. Sun, "Piezoelectrically driven silicon microgrippers integrated with sidewall piezoresistive sensor," in Robotics and Automation, 2009. ICRA '09. IEEE International Conference on, 2009, no. 2006, pp. 2989–2994.

viii. R. K. Messenger, Q. T. Aten, T. W. McLain, and L. L. Howell, "Piezoresistive Feedback Control of a MEMS Thermal Actuator," Microelectromechanical Syst. J., vol. 18, no. 6, pp. 1267–1278, 2009.

ix. R. Conant and R. Muller, "Cyclic fatigue testing of surface-micromachined thermal actuators," Proc. ASME Micro-Electro-Mechanical Syst. ASME Winter Int. Congr. Expo., vol. 66, pp. 273 –277, 1998.

x. S. Muratet, S. Lavu, J.-Y. Fourniols, G. Bell, and M. P. Y. Desmulliez, "Reliability modelling and analysis of thermal MEMS," J. Phys. Conf. Ser., vol. 34, no. 1, pp. 235–240, Apr. 2006.

xi. S. T. Todd, "Electrothermomechanical modeling of a 1-D electrothermal MEMS micromirror," University of Florida, 2005.

xii. F. Fields and H. Hammer, "Analytical Model for Comb-Capacitance Fringe Fields," Microelectromechanical Syst. J., vol. 19, no. 1, pp. 175–182, 2010.

xiii. R. Legtenberg, "Comb-drive actuators for large displacements," ... Micromechanics ..., vol. 6, no. 3, pp. 320–329, Sep. 1996.

xiv. M. A. Hopcroft, W. D. Nix, and T. W. Kenny, "What is the Young's modulus of silicon?," J. Microelectromechanical Syst., vol. 19, pp. 229–238, 2010.